Journal of Molecular Structure 1321 (2025) 140194

Contents lists available at ScienceDirect

Journal of Molecular Structure

journal homepage: www.elsevier.com/locate/molstr

Experimental and theoretical approaches to structural, spectroscopic, electronic and NLO properties of a herbicide fentrazamide

Semiha Bahçeli [a,*], Halil Gökce [b,*]

[a] Department of Astronautical Engineering, Faculty of Aeronautics and Astronautics, University of Turkish Aeronautical Association, Ankara, Turkey
[b] Vocational School of Health Services, Department of Medical Services and Techniques, Giresun University, Giresun, Turkey

ARTICLE INFO

Keywords:
Fentrazamide
DFT/B3LYP
Molecular structure
Molecular spectroscopy
Electronic properties
NLO response

ABSTRACT

A herbicide fentrazamide which is a chemical class tetrazolinone derivative was studied by using FT-IR, ^{1}H- and ^{13}C-NMR (in chloroform-*d*) and UV–Vis. (in acetonitrile) spectroscopic techniques. To support the experimental spectral data and to uncover electronic structure properties, the compound was theoretically modeled at the DFT/B3LYP method with the 6–311++*G*(d,p) basis set. The molecular structural parameters (bond lengths and angles) and harmonic vibrational wavenumbers were obtained in the gas phase at the ground state of the compound. Theoretical NMR chemical shifts were investigated with GIAO method. The intra-molecular electronic transition features were detailed with the help of the computational UV–Vis. spectral and HOMO-LUMO analyses. The presence and species of the intra-molecular hyperconjugative interactions were studied by NBO study. Moreover, the natural and Mulliken atomic charges were determined with the computational method. The electrophilic and nucleophilic reactive attack sites of fentrazamide were determined with the theoretical simulation of its MEPS surface map. To gain insight into the NLO behavior of fentrazamide, the polarizability (α) and hyperpolarizability (β for first-order and γ for second-order) values were calculated at the static and dynamic (ω = 532 nm and 1064 nm) states. The thermodynamic profile of the compound was theoretically analyzed.

1. Introduction

In agriculture, one of the most important issues for grain producers is to improve the quality of the crop and increase the yield. According to 2012 data, the rice is the second largest produced grain plant in the world since it is a principal food for over 60 % of the world and 70 % of Indian population [1]. However, we can easily state that the weeds such as sedges, barnyards, various grasses in paddy rice cultivation or in transplanted rice give rise to reduce the rice production very seriously [2–5]. Undoubtedly, in the face of this situation, the use of herbicide was inevitable against the weeds which are a main threat for rice producers. However, instead of the old known herbicides, a novel and safer herbicide with more effective and eco- friendly and used in low doses was preferred to develop. In this framework, the fentrazamide (or 4-(2-Chlorophenyl)-*N*-cyclohexyl-*N*-ethyl-4,5-dihydro-5-oxo-1*H*-tetrazole-1-carboxamide, IUPAC name; 4-(2-chlorophenyl)-*N*-cyclohexyl-*N*-ethyl-5-oxotetrazole-1-carboxamide) was discovered and developed by Bayer AG and Nihon Bayer Agro-chem [6–9]. The fentrazamide is still called rice herbicide with a new chemical structure [10]. The potential of fentrazamide as a herbicide, along with its molecular structure, effects on weed control in rice fields, comparisons with existing herbicides and environmental safety factors have been revealed through laboratory tests and field trials [11,12]. These aspects highlight its agricultural relevance and sustainability. Fentrazamide has emerged as a focal point in agricultural research, particularly due to its effects on aquatic plants and rice ecosystems. On the other hand, the investigations on the phytotoxic symptoms of fentrazamide also indicate the property of inhibiting cell division [13–16]. Lim et al. [17] investigated the processes of absorption, translocation and metabolism of this compound in rice and early watergrass, highlighting its potential benefits in crop protection practices. Furthermore, in another study, they investigated the effect of the compound on protein metabolism and cell division, which is critical for understanding its role in plant growth and development [13]. Additionally, Goto et al. [18] addressed the advantages of fentrazamide compared to other herbicides and discussed selection criteria, contributing to the development of effective pest management strategies. Together, these studies underscore the significance of fentrazamide not only as an effective herbicide but also as a component that influences plant metabolism, thereby laying the groundwork for sustainable agricultural practices. Consequently,

* Corresponding authors.
E-mail addresses: s.bahceli.81@gmail.com (S. Bahçeli), halil.gokce@giresun.edu.tr, halilgokce.hg@gmail.com (H. Gökce).

https://doi.org/10.1016/j.molstruc.2024.140194
Received 22 August 2024; Received in revised form 21 September 2024; Accepted 25 September 2024
Available online 26 September 2024

fentrazamide is a vital subject of research in agricultural science, offering insights into both its efficacy and potential applications. Tandon et al. [19] have investigated how fentrazamide dissipates in soil under anaerobic conditions, how long it persists, and how microbial metabolic reactions affect the degradation process of this chemical. Similarly, they studied demonstrating how fentrazamide degrades in soil under aerobic conditions, showing that microorganisms work more efficiently to break down this chemical more rapidly [20]. Both studies highlight the impact of fentrazamide on soil quality and ecosystem health, which is crucial for environmental sustainability. Therefore, understanding the behavior of fentrazamide in soil is important for ensuring its safe and effective use in agricultural practices.

We focus on a herbicide fentrazamide by examining both experimentally (using spectroscopic techniques) and theoretically (by quantum chemical calculation methods) since there is no its study in the literature up to now with our best knowledge. Therefore, at this present work, the experimental characterization of fentrazamide were performed with help of the vibrational (FT-IR), ^{1}H- and ^{13}C-NMR and UV–Vis. electronic absorbance spectroscopies, while the computational analyses on the optimize molecular geometry, vibrational wavenumbers and their assignments, proton and carbon-13 NMR chemical shift data, UV–Vis. spectral parameters, HOMO-LUMO energies and simulations, NBO analysis, natural and Mulliken atomic charges, molecular electrostatic potential (MESP) surface, static and dynamic NLO response and thermochemical investigation were carried out at the B3LYP/6–311++*G*(d,p) level of the theory.

2. Experimental details

Fentrazamide compound, which is used as a herbicide, was purchased from a commercial company (Sigma-Aldrich, 99.8 %) and was used without any further purification operation. For the compound at solid powder form, the Perkin-Elmer Spectrum Two FT-IR Spectrometer was used to record Fourier Transform Infrared (FT-IR) spectrum in the region of 400–4000 cm^{-1}. The spectral resolution of FT-IR spectrum is 2 cm^{-1}. To obtain the carbon-13 and proton NMR chemical shift spectra, the fentrazamide was dissolved in chloroform-*d*. The NMR spectral measurements were performed using Bruker Biospin-Avance III 400 MHz NMR spectrometer. The NMR chemical shift spectra were obtained at 100 MHz (for carbons) and 400 MHz (for protons) in ppm relative to tetramethylsilane (TMS). The UV–Vis. spectrum of fentrazamide dissolved in acetonitrile was recorded on a UV-6100 Dual Beam Spectrophotometer in the spectral range 190–1100 nm with a spectral bandwidth of 2 nm.

3. Computational details

Theoretical modeling on the optimized molecular structure features, vibrational wavenumbers, NMR chemical shifts, UV–Vis. spectral parameters, HOMO-LUMO simulations, NBO analysis, atomic charges, static and dynamic non-linear optical (NLO) quantities and thermochemistry investigation of fentrazamide were achieved with the DFT/B3LYP/6–311++*G*(d,p) computational level [21,22]. The Gaussian 09 W [23] and GaussView5 [24] softwares were used for the quantum mechanical computations and their visualizations, respectively. The theoretical harmonic vibrational frequencies were scaled with 0.983 (below 1700 cm^{-1}) and 0.958 (above 1700 cm^{-1}) [25]. The vibrational assignments for these wavenumbers were analyzed with the VEDA4xx software [26,27]. To compute the NMR and UV–Vis. spectroscopic data, the structural geometry of fentrazamide was re-optimized in chloroform and acetonitrile solvents with the IEFPCM solvation model [28], respectively. Based on the optimized structural geometric forms, the carbon-13 and proton NMR chemical shift values and UV–Vis. spectral parameters were computed by the GIAO and TD-DFT methods [29–32]. The HOMO-LUMO simulations were investigated within acetonitrile. The intra-molecular hyperconjugative interactions were revealed by NBO study. Mulliken and natural charges were investigated in the gas phase of the compound. The MESP surface was mapped to determine the electrophilic and nucleophilic reactive attack sites of fentrazamide. The polarizabilities (α), first-order hyperpolarizability (β) and second-order hyperpolarizability (γ) quantities at the static and dynamic (ω = 532 and 1064 nm) states were theoretically obtained to evaluated the NLO response of fentrazamide. The numerical analysis of the computed polarizabilities was performed with the Multiwfn software [33]. Finally, the thermochemistry study was performed under the standard conditions in the gas phase of the molecule.

4. Results and discussion

4.1. Optimized molecular structure analysis

In order to determine the most stable conformational form of fentrazamide, the scan or potential energy surface (PES) analysis was performed with the HF/LanL2DZ computational level. The C4-C3-N24-N23 (6 steps, 60°), C1-N21-C2-N20 (24 steps, 15°) and N21-C2-N20-C10 (9 steps, 45°) dihedral angles were determined as scan coordinates. The total molecular electronic energy value for the most stable conformational form is −1053.814149 Hartree. The PES formed for fentrazamide were depicted Figure S1 (Supplementary Material). By using the initial structure coordinates of the most stable conformational form, the re-optimized molecular geometry and geometrical parameters of fentrazamide were determined with the B3LYP/6–311++*G*(d,p) computational level. The optimized molecular structural form depicted in Fig. 1 of fentrazamide has total molecular electronic energy of −1506.438755 Hartree. The optimized geometrical data (bond length and angles) were given in Table 1. The bond lengths within 5-oxotetrazole group of fentrazamide were computed as 1.2099 Å for the C1=O19, 1.2617 Å for the N22=N23, 1.3702/1.3729 Å for the N23-N24/N21-N24 and 1.3925/1.3956 Å for the C1-N24/C1-N21. In the literature, similar theoretical geometrical data were recorded at the B3LYP/6–31G* level for two nitrogen-rich energetic materials 1,4-diaminotetrazol-5-one (DATO) and 1,4-dinitrotetrazol-5-one (DNTO) [34]. Moreover, the experimental and computational structural results of some compounds based on tetrazol-5-one in the literature are in a good agreement with the geometric data of the same molecular group within our compound [35–37]. The C2=O18 and C2-N20 bond lengths within the carboxamide group were found at 1.2115 Å and 1.3502 Å in our computations, respectively. The bond lengths between atoms bonded to the carbon and nitrogen atoms in this group were calculated as 1.4675 Å for the C2-N21, 1.4828 Å for the C10-N20 and 1.4783 Å for the C16-N20. The C3-N24 bond length connecting 5-oxotetrazole and 2-chlorophenyl rings was calculated as 1.4204 Å. Among the molecular bonds of fentrazamide, the longest bond belongs to the C4-Cl9 with a

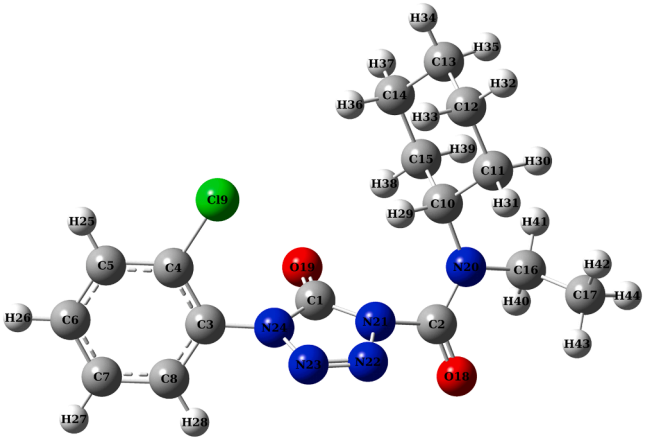

Fig. 1. The optimized molecular structure of fentrazamide.

Table 1
The optimized molecular structure parameters of fentrazamide.

Bond lengths (Å)	Calc.	Bond angles (°)	Calc.	Bond angles (°)	Calc.
C1-O19	1.2099	O19-C1-N21	129.96	C14-C13-H35	109.33
C1-N21	1.3956	O19-C1-N24	129.58	H34-C13-H35	106.50
C1-N24	1.3925	N21-C1-N24	100.46	C13-C14-C15	111.82
C2-O18	1.2115	O18-C2-N20	126.00	C13-C14-H36	109.51
C2-N20	1.3502	O18-C2-N21	118.27	C13-C14-H37	110.43
C2-N21	1.4675	N20-C2-N21	115.72	C15-C14-H36	109.10
C3-C4	1.3987	C4-C3-C8	119.63	C15-C14-H37	109.50
C3-C8	1.3946	C4-C3-N24	120.99	H36-C14-H37	106.32
C3-N24	1.4204	C8-C3-N24	119.38	C10-C15-C14	110.75
C4-C5	1.3917	C3-C4-C5	120.19	C10-C15-H38	108.99
C4-Cl9	1.7488	C3-C4-Cl9	120.64	C10-C15-H39	109.86
C5-C6	1.3919	C5-C4-Cl9	119.16	C14-C15-H38	110.55
C5-H25	1.0822	C4-C5-C6	119.70	C14-C15-H39	108.88
C6-C7	1.3936	C4-C5-H25	119.40	H38-C15-H39	107.76
C6-H26	1.0837	C6-C5-H25	120.90	C17-C16-N20	114.07
C7-C8	1.3901	C5-C6-C7	120.45	C17-C16-H40	109.65
C7-H27	1.0831	C5-C6-H26	119.33	C17-C16-H41	110.54
C8-H28	1.0831	C7-C6-H26	120.22	N20-C16-H40	107.59
C10-C11	1.5388	C6-C7-C8	119.72	N20-C16-H41	107.20
C10-C15	1.5391	C6-C7-H27	120.40	H40-C16-H41	107.55
C10-N20	1.4828	C8-C7-H27	119.88	C16-C17-H42	111.65
C10-H29	1.0895	C3-C8-C7	120.31	C16-C17-H43	110.70
C11-C12	1.5373	C3-C8-H28	118.63	C16-C17-H44	109.35
C11-H30	1.0962	C7-C8-H28	121.06	H42-C17-H43	108.85
C11-H31	1.0942	C11-C10-C15	111.41	H42-C17-H44	108.07
C12-C13	1.5346	C11-C10-N20	112.03	H43-C17-H44	108.12
C12-H32	1.0944	C11-C10-H29	107.06	C2-N20-C10	125.55
C12-H33	1.0975	C15-C10-N20	112.20	C2-N20-C16	115.05
C13-C14	1.5343	C15-C10-H29	107.57	C10-N20-C16	119.40
C13-H34	1.0946	N20-C10-H29	106.19	C1-N21-C2	127.40
C13-H35	1.0979	C10-C11-C12	110.70	C1-N21-N22	110.88
C14-C15	1.5365	C10-C11-H30	109.83	C2-N21-N22	118.16
C14-H36	1.0969	C10-C11-H31	109.65	N21-N22-N23	108.86
C14-H37	1.0942	C12-C11-H30	109.05	N22-N23-N24	108.61
C15-H38	1.0913	C12-C11-H31	110.45	C1-N24-C3	127.13
C15-H39	1.0967	H30-C11-H31	107.08	C1-N24-N23	111.03
C16-C17	1.5304	C11-C12-C13	111.76	C3-N24-N23	121.63
C16-N20	1.4783	C11-C12-H32	109.55	C4-C3-N23-N24	111.25
C16-H40	1.0917	C11-C12-H33	109.19	C1-N21-C2-N20	73.69
C16-H41	1.0896	C13-C12-H32	110.50	N21-C2-N20-C10	2.92
C17-H42	1.0919	C13-C12-H33	109.31	N21-C2-N20-C16	−176.73
C17-H43	1.0903	H32-C12-H33	106.38	C2-N20-C10-C11	120.24
C17-H44	1.0939	C12-C13-C14	111.25	C2-N20-C16-C17	−76.50
N21-N22	1.3702	C12-C13-H34	110.10	O19-C1-N21-C2	−18.20
N22-N23	1.2617	C12-C13-H35	109.23	N22-N21-C2-O18	50.16
N23-N24	1.3729	C14-C13-H34	110.31	N21-N22-N23-N24	1.67

value of 1.7488 Å. Other long bond formations occurred between the C—C bonds of *N*-cyclohexyl and *N*-ethyl groups at values of 1.5346–1.5391 Å and 1.5304 Å, respectively, respectively. The C—C bond lengths within 2-chlorophenyl rings were found at the interval of 1.3901–1.3987 Å. The C4-C3-N23-N24, C1-N21-C2-N20, N21-C2-N20-C10, N21-C2-N20-C16, C2-N20-C10-C11 and C2-N20-C16-C17 dihedral angles were obtained at values of 111.25°, 73.69°, 2.92°, −176.73°, 120.24° and −76.50°, respectively.

4.2. Vibrational wavenumbers analysis

The vibrational bands of fentrazamide were studied by the experimental FT-IR spectroscopy and the computational harmonic wavenumbers analyses. The experimental vibrational frequencies, calculated wavenumbers and IR intensities and their corresponding vibrational assignments were summarized in Table 2. The measured and simulated IR spectra were depicted in Fig. 2. Both IR and Raman modes are active for all 126 vibrational motions (3*N*-6) of fentrazamide ($N = 44$ atoms), which has the lowest symmetry C_1 point group.

The aromatic compounds with the sp^2 hybrid cause vibrational bands in 3000–3100 cm^{-1} region due to the CH stretching modes, while the methylene and methyl groups in aliphatic and sigma-bonded ring structures with the sp^3 hybrid give symmetric and asymmetric stretching vibrations in the region below 3000 cm^{-1} [38–41]. In our study, the weak intensity absorption bands observed at 3047, 3073 and 3101 cm^{-1} in the experimental IR spectrum of fentrazamide were attributed to the CH stretching modes in the 2-chlorophenyl ring. The computed values corresponding to these bands were found to be 3045.1, 3067.3 and 3072.2 cm^{-1}. Similarly, the methylenes and methyl within *N*-cyclohexyl and *N*-ethyl groups of fentrazamide gave vibrational absorption bands at 2856, 2879, 2933, 2969, 2986 and 3000 cm^{-1} as the experimental and 2873.6, 2909.7, 2924.9, 2969.7, 2976.4 and 3000 cm^{-1} as the computational. The in-plane and out-of-plane bending vibrational modes of the 2-chlorophenyl were found at 1439 (exp.)/1450.1 (calc.), 1261 (exp.)/1257.1 (calc.), 1178 (exp.)/1167.9 (calc.), 1146 (exp.)/1164.9 (calc.) and 1136 (exp.)/1133.0 (calc.) cm^{-1} and 963 (exp.)/952.8 (calc.), 958 (exp.)/943.9 (calc.), 863 (exp.)/862.7 (calc.) and 756 (exp.)/761.9 (calc.) cm^{-1}, respectively. The scissoring (δ_s), wagging (w), twisting (t) and rocking (ρ) modes of *N*-cyclohexyl and *N*-ethyl groups were listed in Table 2.

The compounds containing carbonyl group (C = O) strong generate vibrational absorption bands in the region of 1740–1870 cm^{-1} [38–41]. The 5-oxotetrazole and 1-carboxamide groups in our compound formed the strong absorption bands at 1706 and 1751 cm^{-1} in the experimental FT-IR spectrum due to the C1=O19 and C2=O18 stretching modes, respectively. The computed wavenumber values were found at 1732.1 cm^{-1} (PED-82 %) for the C1=O19 stretching mode and 1695.8 cm^{-1} (PED-79 %) for the C2=O18 one. The N22=N23 stretching band within 5-oxotetrazole group was obtained at 1452 cm^{-1} as the experimental and 1459.7 cm^{-1} with contribution 67 % of PED as the computational. The CN and NN stretching vibrational modes in the same group were experimentally obtained at 958, 1122, 1146 and 1178 cm^{-1} in combination with each other and other vibrational bands, while they were theoretically computed at 943.9, 1111.3, 1164.9 and 1167.9 cm^{-1}. The C=O, NN and CN vibrational frequency values obtained for this group in the experimental and computational studies of some molecular systems containing tetrazol-5-one (5-oxatetrazole) group in the literature are in agreement with the values presented in our study [34–37,42]. The C_2N_{20} stretching band in the 1-carboxamide group appeared at 1422 (exp.)/1420.50 (calc.) cm^{-1} as mixed with other vibrational modes. The ring CC stretching bands of the aromatic 2-chlorophenyl were found at 1590 (exp.)/1602.7 (calc.), 1581(exp.)/1587.9 (calc.), 1490 (exp.)/1492.9 (calc.), 1439(exp.)/1453.1 (calc.) and 1307(exp.)/1296.3 (calc.) cm^{-1}. Likewise, the *N*-cyclohexyl group gave the absorption bands at 816, 1029 and 1075 cm^{-1} as the experimental and 803.9, 1022.3 and 1072.7 cm^{-1} as the theoretical. The other vibrational bands such as the CN stretching modes and the deformation modes of the aromatic and sigma-bonded rings, etc. in fentrazamide were also presented in Table 2.

Table 2
The experimental and computed vibrational frequencies and their vibrational assignments of fentrazamide.

Vibrational assignments (PED%≥ 10)	Exp. IR (cm^{-1})	Unscaled freq.	Scaled freq.	I_{IR}
νCCl(15)+δCCCl(14)	429	435.1	427.7	6.54
δCCC(30) in *N*-ch.	437	438.2	430.8	0.71
$\delta O_{18}C_2N_{21}(14)$+δCCC(11) in *N*-ch.	451	456.6	448.9	0.22
γCCCCl(25)+τCCCC(21) in 2-cp.	463	472.3	464.2	3.98
δCCC(12) in *N*-ch.	492	487.2	478.9	3.38
$\delta C_8C_3N_{24}(23)$+τCCCC(11) in 2-cp.	497	497.9	489.5	4.63
δCCC(30) in *N*-ch.	517	511.3	502.6	4.13
τCCCC(21) in 2-cp.+δ $C_{17}C_{16}N_{20}(12)$	532	540.4	531.2	4.64
τCCCC(13) in 2-cp.	542	557.7	548.2	3.55
$\delta O_{19}C_1N_{24}(17)$+τNNNN(12) in 5-ot.	617	621.9	611.3	1.98
δCCC(63) in 2-cp.+τNNNN(10) in 5-ot.	663	675.8	664.3	9.34
τNNNN(53) in 5-ot.	680	694.3	682.5	12.20
$\gamma O_{19,18}N_{21,20}N_{24,21}C_{1,2}(19)$+τ CCCC(16) in 2-cp.	719	728.2	715.8	11.43
$\gamma O_{19,18}N_{21,20}N_{24,21}C_{1,2}(26)$+τ CCCC(14) in 2-cp.	728	737.9	725.3	3.68
$\gamma O_{19,18}N_{21,20}N_{24,21}C_{1,2}(25)$+τ CCCC(15) in 2-cp.	744	756.7	743.8	35.28
τHCCC(54) in 2-cp.	756	775.1	761.9	38.58
$\rho CH_{2,3}(26)$ in *N*-ethyl	771	785.3	771.9	7.98
$\rho CH_2(11)$ in *N*-ch.	784	797.4	783.9	11.03
νCC(64) in *N*-ch.	816	817.8	803.9	7.75
$\nu C_{16}N_{20}(13)$	852	866.2	851.5	36.75
τHCCC(78) in 2-cp.	863	877.6	862.7	4.72
[νCC(37)+$\rho CH_2(11)$] in *N*-ch.	892	903.6	888.2	6.27
$\rho CH_2(11)$ in 5-ot.	908	916.6	901.0	12.85
[νCC(17)+$\rho CH_2(12)$] in *N*-ch.	918	930.3	914.4	1.43
τHCCC(27) in 2-cp.+[νCN/NN (18)+δNNN(11)] in 5-ot.	958	960.2	943.9	4.99
τHCCC(56) in 2-cp.	963	969.3	952.8	11.06
δCCC(11) in *N*-ch.	975	992.3	975.4	9.23
$\nu C_{16}C_{17}(12)$+$\nu C_{16}N_{20}(12)$+δCCC (10) in *N*-ch.	1010	1022.0	1004.6	18.32
[νCC(32)+δCCC(10)] in *N*-ch.	1029	1040.0	1022.3	6.05
[δCCC(47)+νCC(14)] in 2-cp.	1053	1058.0	1040.0	35.51
νCC(51) in *N*-ch.	1075	1091.3	1072.7	0.13
[δNNN(21)+νNN(11)] in 5-ot.	1093	1102.4	1083.7	124.44
$\rho CH_{2,3}(26)$ in *N*-ethyl	1102	1112.3	1093.4	44.04
[νCC(-)+δHCC(-)] in 2-cp.+[νCN/NN(-)] in 5-ot.	1122	1130.6	1111.3	41.10
[δHCC(40)+νCC(38)] in 2-cp.	1136	1152.6	1133.0	21.15
δHCC(34) in 2-cp.+νNN(27) in 5-ot.	1146	1185.1	1164.9	27.23
δHCC(35) in 2-cp.+νNN(20) in 5-ot.	1178	1188.1	1167.9	21.25
$\nu C_{10}N_{20}(29)$	1204	1223.3	1202.5	33.58
$tCH_2(19)$ in *N*-ch.	1240	1263.5	1242.0	37.16
δHCC(34) in 2-cp.+δNNN(15) in 5-ot.+$\nu C_2N_{21}(11)$	1261	1278.8	1257.1	47.17
[$tCH_2(43)$+$\delta H_{29}CC(11)$] in *N*-ch.	1264	1287.8	1265.9	5.85
$tCH_2(20)$ in *N*-ch.	1293	1294.0	1272.0	92.84
νCC(75) in 2-cp.	1307	1318.8	1296.3	10.70
[$\delta H_{29}CC(30)$+*w*,$tCH_2(10)$] in *N*-ch.	1334	1354.8	1331.7	5.23
w,$tCH_2(51)$ in *N*-ch.	1352	1378.3	1354.9	5.01
[w,$tCH_2(43)$+$\delta H_{29}CC(10)$] in *N*-ch.	1359	1384.9	1361.3	7.64
$\nu C_3N_{24}(27)$	1374	1393.6	1369.9	66.38
[$wCH_2(21)$+$\delta_s CH_3(15)$ (*sym.* bending)] in *N*-ethyl	1407	1409.6	1385.6	4.66
$\nu C_2N_{20}(-)$+$\delta H_{29}CC(-)$ in *N*-ch.+ $tCH_2(-)$ in N-ethyl	1422	1445.1	1420.5	80.28
[δHCC(46)+νCC(28)] in 2-cp.	1439	1475.1	1450.1	18.42
$\nu N_{22}{=}N_{23}(67)$	1452	1484.9	1459.7	37.57
$\delta_s CH_2(59)$ in *N*-ch.+$\delta_s CH_{2,3}(17)$ in *N*-ethyl	1470	1496.8	1471.3	23.12
[δCCC(34)+νCC(16)] in 2-cp.	1490	1518.7	1492.9	70.67
[νCC(58)+δCCC(21)] in 2-cp.	1581	1615.4	1587.9	5.44
[νCC(53)+δHCC(16)] in 2-cp.	1590	1630.5	1602.7	4.51

Table 2 (*continued*)

Vibrational assignments (PED%≥ 10)	Exp. IR (cm^{-1})	Unscaled freq.	Scaled freq.	I_{IR}
$\nu O_{18}{=}C_2(79)$	1751	1770.2	1695.8	506.22
$\nu O_{19}{=}C_1(82)$	1706	1808.0	1732.1	374.69
$\nu_s CH_2(89)$ in *N*-ch.	2856	2999.6	2873.6	16.23
$\nu_s CH_3(89)$ in *N*-ethyl	2879	3037.3	2909.7	29.43
$\nu_{as} CH_2(79)$ in *N*-ch.	2933	3053.2	2924.9	60.28
[$\nu_{as} CH_3(77)$+$\nu_s CH_2(20)$] in *N*-ethyl	2969	3099.9	2969.7	28.64
νCH(50) in *N*-ch.+$\nu_{as} CH_{2,3}(26)$ in *N*-ethyl	2986	3106.9	2976.4	23.42
$\nu_{as} CH_{2,3}(91)$ in *N*-ethyl	3000	3131.5	3000.0	20.32
νCH(97) in 2-cp.	3047	3178.6	3045.1	1.36
νCH(95) in 2-cp.	3073	3201.8	3067.3	2.26
νCH(83)in 2-cp.	3101	3206.9	3072.2	2.83

s, symmetric; as, asymmetric; ν, stretching; δ, in-plane bending; τ, torsion; γ, out-of-plane bending; δ_s, scissoring and symmetric bending; ρ, rocking; t, twisting; w, wagging; I_{IR}, IR intensity (km mol^{-1}); PED, potential energy distribution; 2-cp., 2-chlorophenyl; *N*-ch., *N*-cyclohexyl; 5-ot., 5-oxotetrazole.

4.3. NMR chemical shifts analysis

The experimental ^{13}C- and ^{1}H-NMR spectroscopic records of fentrazamide were taken in chloroform-*d* ($CDCl_3$) and presented in Fig. 3. By using IEFPCM model and chloroform solvent, the computational chemical shift analyses values of the carbon and hydrogen nucleus of the compound were performed with GIAO method at the B3LYP/6–311++*G*(d,p) level. The experimental records and theoretical data for the NMR chemical shifts of the hydrogen and carbon nucleus in fentrazamide were given in Table 3.

The carbonyl carbon atoms (C1 and C2) in the oxotetrazole and carboxamide groups gave a resonance signal at 147.3 ppm in the higher chemical shift region of the experimental carbon-13 NMR spectrum due to the electronegative effect of the oxygen atom. The theoretical values computed for these carbons were found at 154.9 and 154.8 ppm. The sp^2 hybrid aromatic carbons (C3, C4, C5, C6, C7 and C8) of 2-chlorophenyl group were obtained at the intervals of 128.1–131.9 ppm as the experimental and 135.2–150.0 ppm as the theoretical. The carbons (C10, C11, C12, C13, C14 and C15) in *N*-cyclohexyl, another ring structure, resonated in the lower chemical shift region because they are shielded by their own hydrogen. The strong signal observed at 25.8 ppm in the experimentally recorded NMR chemical shift spectrum can be attributed to the C11, C12, C14 and C15 carbons. The NMR resonance signal of the C13 carbon were observed at 31.7 ppm, while the C10 carbon atom bonded to the heteroatom N20 nitrogen atom resonated at 59.8 ppm. These carbons gave theoretical results at the internal of 30.1–66.4 ppm. The C16 and C17 carbons within the *N*-ethyl group were obtained at 39.2/45.0 ppm (exp./calc.) and 14.1/15.4 ppm (exp./calc.), respectively. The protons on aromatic carbons with sp^2 hybrid gave the experimental and theoretical resonance signals in the ranges 7.45–7.62 ppm and 7.72–7.87 ppm. The protons in other groups (*N*-cyclohexyl and *N*-ethyl) were measured/computed at 4.09/3.62 ppm, 1.54–1.97/1.56–2.20 ppm, 3.50/3.21–3.62 ppm and 1.14–1.33/0.99–1.94 ppm.

4.4. UV–Vis. spectral analysis

The molecular electronic transition properties can be determined with the experimental and computational investigations of the UV–Vis. spectral research. The measured UV–Vis. spectroscopic record of fentrazamide was obtained in acetonitrile. To support the experimental wavelength records, the computational UV–Vis. study of fentrazamide was performed with the TD-DFT/B3LYP/6–311++*G*(d,p) theoretical level. The experimental wavelength records and computed measured UV–Vis. spectral parameters (electronic absorption wavelengths, excitation energies, oscillator strengths and electronic transitions in HOMOs and LUMOs) were presented in Table 4. the experimental and simulated

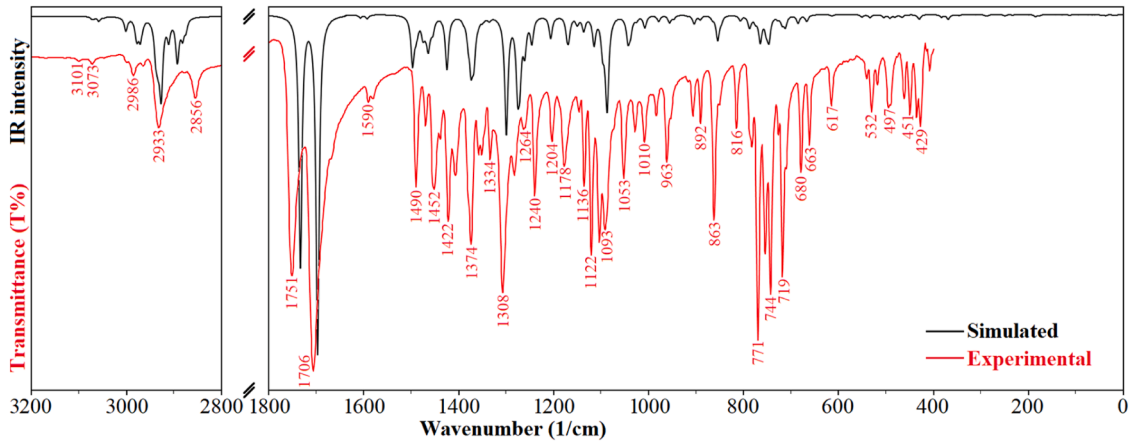

Fig. 2. The experimental (red) and simulated IR spectra of fentrazamide.

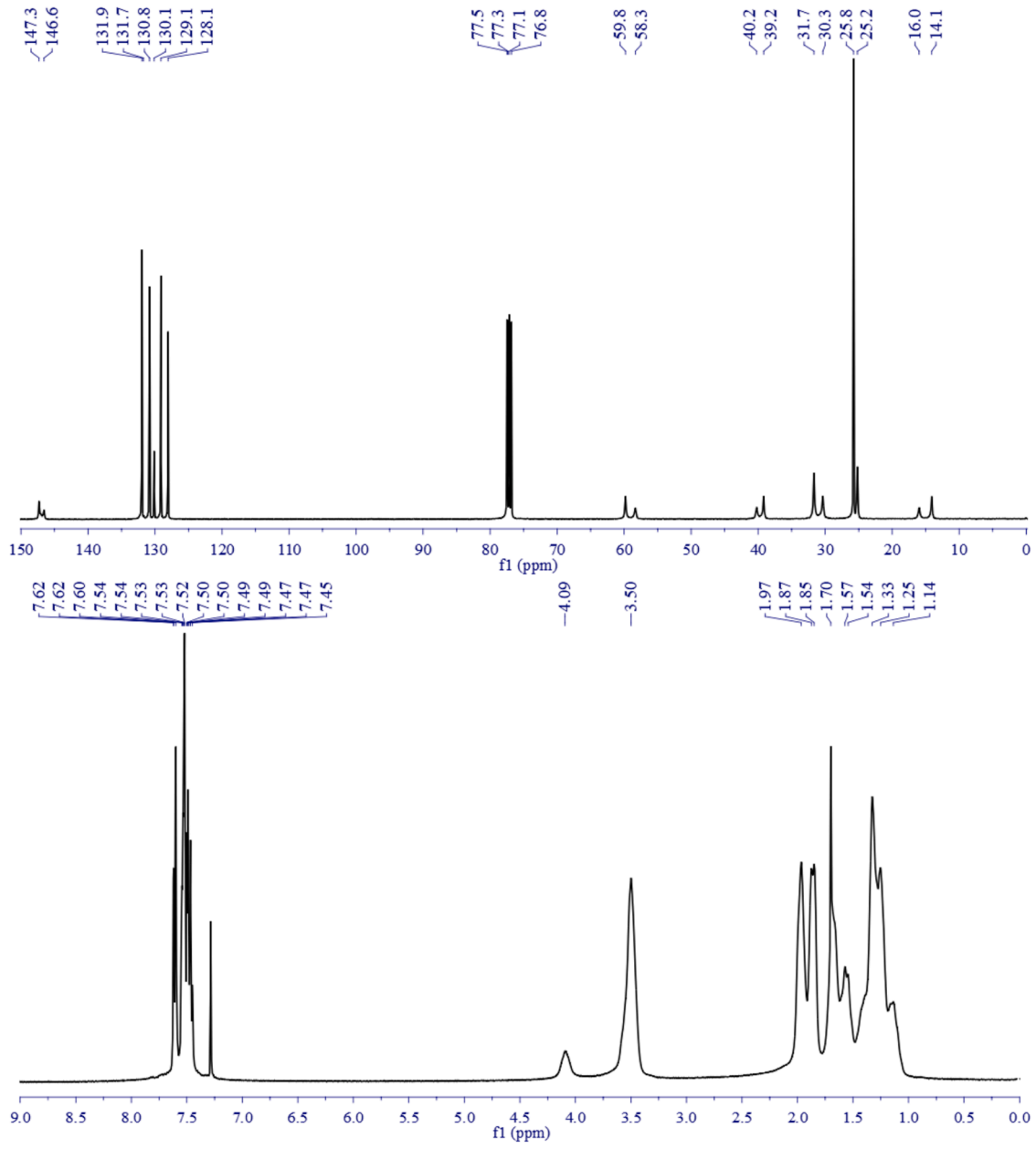

Fig. 3. The experimental ^{13}C (top) and ^{1}H (bottom) NMR chemical shift spectra of fentrazamide.

Table 3
The experimental and computed ^{1}H and ^{13}C NMR isotropic chemical shifts (with respect to TMS, all values in ppm) of fentrazamide.

Atoms	$\delta_{exp.}$	$\delta_{cal.}$	Atoms	$\delta_{exp.}$	$\delta_{cal.}$
C1	147.3	154.9	H25	7.45–7.62	7.87
C2	147.3	154.8	H26		7.86
C3	128.1–131.9	139.1	H27		7.72
C4		150.0	H28		7.74
C5		137.0	H29	4.09	3.62
C6		140.3	H30	1.54–1.97	1.56
C7		135.2	H31		1.82
C8		139.0	H32		1.85
C10	59.8	66.4	H33		1.36
C11	25.8	37.0	H34		1.62
C12		31.5	H35		1.29
C13	31.7	30.1	H36		1.47
C14	25.8	30.7	H37		1.77
C15		34.8	H38		2.20
C16	39.2	45.0	H39		1.56
C17	14.1	15.4	H40	3.50	3.62
			H41		3.21
			H42	1.14–1.33	0.99
			H43		1.94
			H44		1.05

Table 4
The computed and recorded UV–Vis. spectral parameters in ethanol of fentrazamide.

Exp. λ (nm)	Calc. λ (nm)	f	ΔE (eV)	Major contributions
193 (π→π*)	244.46	0.0043	5.0718	H→L (63 %), H-1→*L* + 1 (17 %)
237 (n→π*)	243.17	0.0164	5.0987	H-1→*L* + 1 (38 %), H→L (31 %)
	240.49	0.0265	5.1555	H-1→L (83 %)
	232.87	0.1681	5.3241	H-2→L (80 %)

f, Oscillator strengths; ΔE, Excitation energy; H, HOMO; L, LUMO.

UV–Vis. spectroscopic graphics were given in Fig. 4. The GaussSum 3.0.1 software [43] was used to analyze the major contributions of the electronic transitions from HOMO to LUMO corresponding to each computed UV spectral wavelength.

The electronic absorption wavelengths emerged at 193 and 237 nm on the experimental UV–Vis. spectroscopic wavelength-absorbance graphic may be due to π→π* or n→π* electronic transitions. These transitions may be resulted from bond formations (C=O and *N* = *N*) and lone pair electrons of the nitrogen and oxygen heteroatoms within the carboxamide and oxotetrazole groups of fentrazamide [44]. Four electronic absorption wavelengths computed for fentrazamide were found at 244.46, 243.17, 240.49 and 232.87 nm. The oscillator strengths of these values were obtained at 0.0043, 0.0164, 0.0265 and 0.1682, respectively. The HOMO→LUMO, the most probable transition in a molecular system, has a major contribution of 63 % and 31 % at 244.46 nm and 243.17 nm. The electronic transition corresponding to 232.87 nm, where the oscillator strength is strongest, belongs to the H-2→L transition with 80 % value of the major contribution.

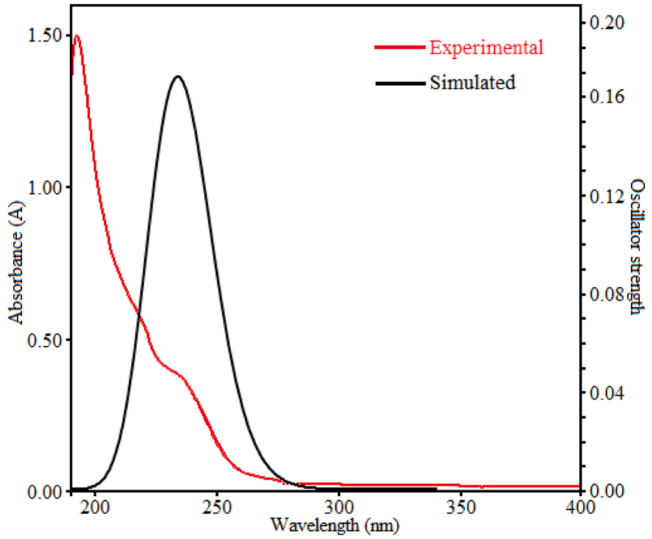

Fig. 4. The experimental (red) and simulated (black) UV spectra of fentrazamide.

4.5. FMO analysis

Frontier molecular orbitals (FMOs), which are used to investigate the chemical reactivity of a molecule, focus especially on the analysis of the highest occupied molecular orbitals (HOMOs) and the lowest unoccupied molecular orbitals (LUMOs). If we have the necessary information about the HOMO and LUMO molecular orbitals of a molecular electronic system, many molecular electronic and electrical properties such as electronic transitions, charge transfers, molecular acidity and basicity, chemical stability, kinetic stability, molecular conductivity, electron affinity, ionization potential, chemical potential, chemical hardness and softness, electrophilicity index and electronegativity, etc. of that system can be determined [45–51]. The LUMO+1, LUMO, HOMO, HOMO-1, HOMO-2 and HOMO-3 plots and their energy values simulated with the DFT/B3LYP/6–311++*G*(d,p) level of fentrazamide were presented in Fig. 5. The LUMO and HOMO energy values and the |HOMO-LUMO| energy band gap between them were calculated as −1.562, −7.333 and 5.771 eV, respectively. Depending on LUMO and HOMO simulations, some molecular features computed for fentrazamide were listed in Table 5. The electron affinity ($A = -E_{LUMO}$) and ionization potential ($I = -E_{HOMO}$) values for were found as 1.562 and 7.333 eV, respectively. High value of the energy band gap between HOMO and LUMO leads to a high-energy excitation. This means low molecular chemical reactivity [52]. The electron densities of the LUMO+1 and LUMO simulations were localized on the anti-bonding pi (or π*) molecular orbitals of 2-chlorophenyl and 5-oxotetrazole rings of fentrazamide. The HOMO was mostly formed from lone pair pi electrons (n_{pi}) of the oxygen and nitrogen atoms within the carboxamide group. Moreover, a small part of HOMO also gave the electron localizations on the sigma (σ) bond orbitals of *N*-ethyl and *N*-cyclohexyl groups. The HOMO-1 was mainly placed on the delocalized pi electrons or the pi bonding (π) molecular orbitals of 2-chlorophenyl. The electron densities on the HOMO-2 and HOMO-3 simulations were occurred from the pi bonding (π) (on N22=N23 group) and lone pair pi bonding (n_{pi}) (on O19, N21 and N24 atoms) molecular orbitals of 5-oxotetrazole. The electron localizations on these aforementioned molecular orbitals can indicate that the HOMOs→LUMOs transitions can be n→π* and π→π*. These transitions also confirm the electronic transitions corresponding to the experimental and calculated wavelength values in the UV–Vis. spectroscopic study.

4.6. NBO analysis

The hyperconjugative interactions within fentrazamide were analyzed via natural bond orbitals (NBO). The *E*(2), stabilization energy, presents interaction between donor (*i*) and acceptor (*j*) groups in molecular system and can be calculated with the following equation [53].

$$E(2) = -q_i \frac{F_{ij}^{\ 2}}{\Delta E} = -q_i \frac{\langle i|F|j\rangle^2}{\varepsilon_j - \varepsilon_i}$$

where q_i is the donor orbital occupancy, ε_i and ε_j are the diagonal orbital energy elements of donor and acceptor groups and F_{ij} is the off-diagonal

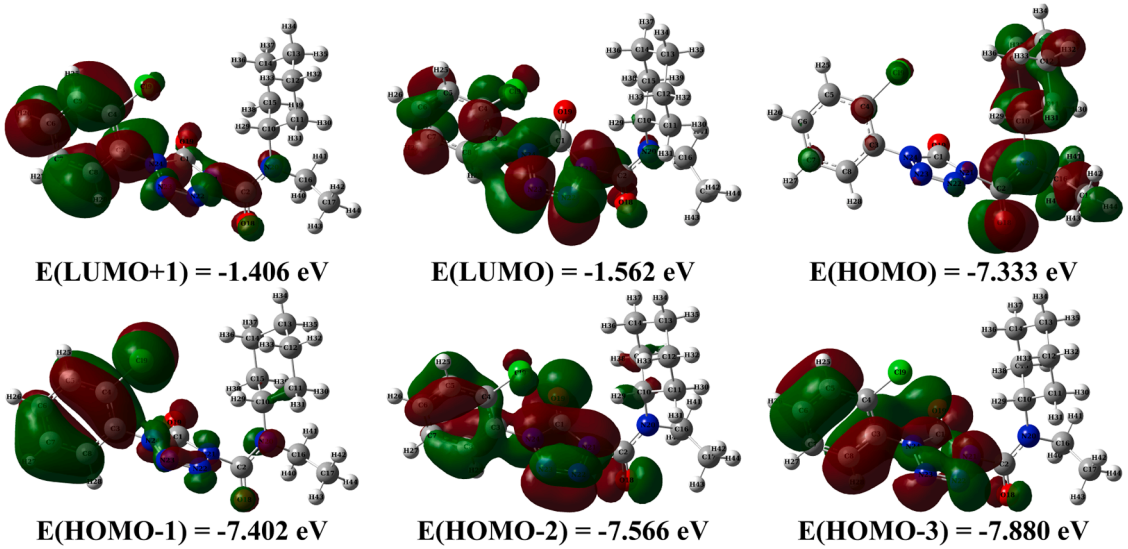

Fig. 5. The LUMO+1, LUMO, HOMO, HOMO-1, HOMO-2 and HOMO-3 simulations of fentrazamide.

Table 5
The global reactivity descriptors computed of fentrazamide.

Parameters (eV)	Values
E_{LUMO}	−1.562
E_{HOMO}	−7.333
Energy band gap $\|E_{HOMO}$-$E_{LUMO}\|$	5.771
Electron affinity (A = -E_{LUMO})	1.562
Ionization potential (I = -E_{HOMO})	7.333
Chemical hardness (η = (I-A)/2)	2.885
Chemical softness ($\zeta = 1/2\eta$)	0.173
Electronegativity ($\chi = (I + A)/2$)	4.448
Chemical potential (μ = -(I + A)/2)	−4.448
Electrophilicity index ($\omega = \mu^2/2\eta$)	3.428
Maximum charge transfer index ($\Delta N_{max.} = -\mu/\eta$)	1.542

NBO Fock matrix element. The NBO analysis results for the hyperconjugative interactions of fentrazamide were obtained using the B3LYP/6–311++G(d,p) level. The interaction values larger than 3 kcal/mol were listed in Table 6.

The hyperconjugative interactions in fentrazamide were formed between the bonding σ, π and n orbitals of donor groups and the antibonding σ* and π* orbitals of acceptor groups. A strong value for the σ→σ* hyperconjugative interaction was found as 5.37 kcal/mol with the BD(1)(C3-C8)→BD*(1)(C3-C4) notation. The BD(1)(N21-N22 and N23-N24)→BD*(2)(C1-O19) notations were corresponded to the σ→π* hyperconjugative interaction with the stabilization energy values of 3.20 and 3.05 kcal/mol, respectively. The strongest π→π* hyperconjugative interactions were occurred between donor-acceptor groups of 2-chlorophenyl ring in fentrazamide. These results were appeared at values of 17.81, 19.22, 22.45, 18.75, 21.89 and 21.19 kcal/mol with the BD(2)(C3-C4)→BD*(2)(C5-C6 and C7-C8), BD(2)(C5-C6)→BD*(2)(C3-C4 and C7-C8) and BD(2)(C7-C8)→BD*(2)(C3-C4 and C5-C6) notations, respectively. The strongest hyperconjugative interactions in fentrazamide were obtained for the n→σ* and n→π*. Accordingly, the n→σ* and n→π* hyperconjugative interactions were emerged at values of 33.07, 46.38 and 50.65 kcal/mol for the LP(2)(O18)→BD*(1)(C2-N21), LP(1)(N21)→BD*(1)(C1-O19) and LP(1)(N24)→BD*(1)(C1-O19) and 69.33, 35.45 and 38.10 kcal/mol for the LP(1)(N20)→BD*(2)(C2-O18), LP(1)(N21)→BD*(2)(N22-N23) and LP(1)(N24)→BD*(1)(N22-N23), respectively.

4.7. Atomic charges analysis

Mulliken and natural atomic charges arise as a result of wavefunction-based Mulliken population analysis (MPA) [54] and natural population analysis (NPA) [55]. Mulliken and natural atomic charges computed with the B3LYP/6–311++G(d,p) theoretical level of fentrazamide were given in Table 7. The most negative values in the natural atomic charges of fentrazamide were appeared at −0.59240 e for the O18 atom and −0.61594 e for the O19 one, which have the highest electronegativity in the molecule. The C2 and C1 carbon atoms bonded to these oxygen atoms have the most positive natural atomic charges with values of +0.83538 e and +0.77955 e, respectively. The N20 (−0.48862 e), N21 (−0.37030 e), N22 (−0.00602 e), N23 (−0.01977 e) and N24 (−0.32287 e) nitrogen atoms, another electronegative atom in fentrazamide, also have the negative natural charges. The C10, C11, C12, C13, C13, C14, C15, C16 and C17 carbon atoms surrounded by positively charged hydrogens have the negative natural charges at values of −0.00479 e, −0.39010 e, −0.37913 e, −0.38179 e, −0.38085 e, −0.39593 e and −0.17253 e, respectively. As it will be noted, since the C10 and C16 carbons are connected to the nitrogen atom N20, which is neither electronegative nor negatively charged, the negative charges of these carbons are less than the other carbon atoms mentioned. Again, the shielding of the C17 carbon atom by three hydrogens increases its natural negative charge compared to other carbons mentioned. Excepting for the C3 carbon bonded to the electronegative and negatively charged N24 nitrogen atom, the other five aromatic carbons (C4, C5, C6, C7 and C8) have the negative natural charge values. The natural charges computed of aromatic carbons were found as +0.10928 e, −0.02004 e, −0.21422 e, −0.17262 e, −0.19683 e and −0.16108 e, respectively. Twenty hydrogen atoms in fentrazamide have the positive natural charges with values between (+0.18622 e)-(+0.23481 e).

4.8. MESP analysis

Molecular electrostatic potential (MESP) map is a shape created by circulating a positive test charge around the molecule. As a result of this process, there will be no distortion in the charge distribution of molecule. In this way, the molecular chemical reactivity of a molecule towards positive or negative charge reactants can be evaluated [56]. Moreover, the MESP map provides information about inter-molecular hydrogen bonding, non-covalent interactions and electrophilic and nucleophilic reactive attack sites of molecule. A MESP surface is mapped in different colors in terms of red-orange-green-light blue-blue. The red-

Table 6
The hyperconjugative interactions calculated with second-order perturbation theory of Fock matrix in NBO of fentrazamide.

ED (i) (e)	Donor (i)	ED (j) (e)	Acceptor (j)	$E(2)$[a] (kcal/mol)	E(j)-E (i)[b] (a.u.)	F(i,j)[c] (a.u.)
1.98103	BD(1) (C1-N21)	0.03570	BD*(1)(C3-N24)	3.99	1.21	0.062
1.98067	BD(1) (C1-N24)	0.11556	BD*(1)(C2-N21)	3.32	1.14	0.056
1.97318	BD(1) (C3-C4)	0.02584	BD*(1)(C3-C8)	4.57	1.29	0.069
1.97318	BD(1) (C3-C4)	0.02478	BD*(1)(C4-C5)	3.43	1.29	0.059
1.68623	BD(2) (C3-C4)	0.31600	BD*(2)(C5-C6)	17.81	0.31	0.066
1.68623	BD(2) (C3-C4)	0.31196	BD*(2)(C7-C8)	19.22	0.31	0.069
1.68623	BD(2) (C3-C4)	0.05028	BD*(1) (N23-N24)	3.94	0.61	0.047
1.96590	BD(1) (C3-C8)	0.04112	BD*(1)(C3-C4)	5.37	1.26	0.074
1.96590	BD(1) (C3-C8)	0.02914	BD*(1)(C4-Cl9)	4.59	0.86	0.056
1.97822	BD(1) (C4-C5)	0.04112	BD*(1)(C3-C4)	3.84	1.28	0.063
1.97822	BD(1) (C4-C5)	0.03570	BD*(1)(C3-N24)	3.93	1.11	0.059
1.97199	BD(1) (C5-C6)	0.02478	BD*(1)(C4-C5)	3.44	1.26	0.059
1.97199	BD(1) (C5-C6)	0.02914	BD*(1)(C4-Cl9)	4.91	0.86	0.058
1.65635	BD(2) (C5-C6)	0.43257	BD*(2)(C3-C4)	22.45	0.26	0.070
1.65635	BD(2) (C5-C6)	0.31196	BD*(2)(C7-C8)	18.75	0.29	0.066
1.97768	BD(1) (C5-H25)	0.04112	BD*(1)(C3-C4)	4.33	1.07	0.061
1.97768	BD(1) (C5-H25)	0.01549	BD*(1)(C6-C7)	3.52	1.10	0.056
1.97959	BD(1) (C6-H26)	0.02478	BD*(1)(C4-C5)	3.55	1.08	0.055
1.97959	BD(1) (C6-H26)	0.01394	BD*(1)(C7-C8)	3.64	1.10	0.057
1.97681	BD(1) (C7-C8)	0.03570	BD*(1)(C3-N24)	4.04	1.09	0.059
1.65078	BD(2) (C7-C8)	0.43257	BD*(2)(C3-C4)	21.89	0.26	0.069
1.65078	BD(2) (C7-C8)	0.31600	BD*(2)(C5-C6)	21.19	0.28	0.070
1.97994	BD(1) (C7-H27)	0.02584	BD*(1)(C3-C8)	3.64	1.08	0.056
1.97994	BD(1) (C7-H27)	0.01652	BD*(1)(C5-C6)	3.68	1.10	0.057
1.97622	BD(1) (C8-H28)	0.04112	BD*(1)(C3-C4)	4.34	1.07	0.061
1.97622	BD(1) (C8-H28)	0.01549	BD*(1)(C6-C7)	3.52	1.10	0.056
1.96798	BD(1) (C10-H29)	0.03153	BD*(1) (C16-N20)	4.47	0.82	0.054
1.97910	BD(1) (C11-C12)	0.04009	BD*(1) (C10-N20)	3.13	0.92	0.048
1.97947	BD(1) (C11-H31)	0.02679	BD*(1) (C10-C15)	3.11	0.87	0.047
1.97997	BD(1) (C13-H34)	0.01324	BD*(1) (C11-C12)	3.07	0.87	0.046
1.97870	BD(1) (C14-C15)	0.04009	BD*(1) (C10-N20)	3.15	0.91	0.048
1.97814	BD(1) (C15-H38)	0.02644	BD*(1) (C10-C11)	3.30	0.86	0.047
1.98019	BD(1) (C16-N20)	0.11556	BD*(1)(C2-N21)	4.25	1.02	0.060
1.98138	BD(1) (C16-H41)	0.07181	BD*(1)(C2-N20)	3.03	0.99	0.049
1.98358	BD(1) (C17-H44)	0.03153	BD*(1) (C16-N20)	4.37	0.81	0.053
1.98359	BD(1) (N21-N22)	0.02058	BD*(2)(C1-O19)	3.20	1.46	0.061
1.98304	BD(1) (N23-N24)	0.02058	BD*(2)(C1-O19)	3.05	1.46	0.060
1.96800	LP(2) (Cl9)	0.04112	BD*(1)(C3-C4)	5.02	0.86	0.059
1.96800	LP(2) (Cl9)	0.02478	BD*(1)(C4-C5)	3.86	0.88	0.052
1.92131	LP(3) (Cl9)	0.43257	BD*(2)(C3-C4)	13.86	0.32	0.065
1.83243	LP(2) (O18)	0.07181	BD*(1)(C2-N20)	21.93	0.73	0.116
1.83243	LP(2) (O18)	0.11556	BD*(1)(C2-N21)	33.07	0.56	0.123
1.82135	LP(2) (O19)	0.10628	BD*(1)(C1-N21)	28.77	0.64	0.124
1.82135	LP(2) (O19)	0.11034	BD*(1)(C1-N24)	28.72	0.65	0.124
1.63772	LP(1) (N20)	0.34007	BD*(2)(C2-O18)	69.33	0.27	0.122
1.63772	LP(1) (N20)	0.02644	BD*(1) (C10-C11)	4.23	0.63	0.051
1.63772	LP(1) (N20)	0.02679	BD*(1) (C10-C15)	4.91	0.63	0.055
1.63772	LP(1) (N20)	0.01284	BD*(1) (C16-C17)	5.43	0.64	0.058
1.63772	LP(1) (N20)	0.01677	BD*(1) (C16-H40)	3.01	0.67	0.044
1.62335	LP(1) (N21)	0.39390	BD*(1)(C1-O19)	46.38	0.32	0.109
1.62335	LP(1) (N21)	0.02092	BD*(1)(C2-O18)	4.42	0.90	0.062
1.62335	LP(1) (N21)	0.34007	BD*(2)(C2-O18)	11.18	0.32	0.054
1.62335	LP(1) (N21)	0.07181	BD*(1)(C2-N20)	3.54	0.78	0.051
1.62335	LP(1) (N21)	0.32029	BD*(2) (N22-N23)	35.45	0.26	0.086
1.94376	LP(1) (N22)	0.10628	BD*(1)(C1-N21)	5.63	0.85	0.062
1.94376	LP(1) (N22)	0.05028	BD*(1) (N23-N24)	7.69	0.78	0.069
1.94712	LP(1) (N23)	0.11034	BD*(1)(C1-N24)	5.46	0.85	0.062
1.94712	LP(1) (N23)	0.04057	BD*(1) (N21-N22)	7.39	0.80	0.069
1.62066	LP(1) (N24)	0.39390	BD*(1)(C1-O19)	50.65	0.31	0.112
1.62066	LP(1) (N24)	0.04112	BD*(1)(C3-C4)	5.17	0.83	0.064
1.62066	LP(1) (N24)	0.43257	BD*(2)(C3-C4)	3.20	0.29	0.027
1.62066	LP(1) (N24)	0.02584	BD*(1)(C3-C8)	5.25	0.84	0.065

(*continued on next page*)

Table 6 (*continued*)

ED (i) (e)	Donor (i)	ED (j) (e)	Acceptor (j)	$E(2)$[a] (kcal/mol)	$E(j)$-E (i)[b] (a.u.)	$F(i,j)$[c] (a.u.)
1.62066	LP(1) (N24)	0.32029	BD*(2) (N22-N23)	38.10	0.25	0.088

ED is the electron density.
[a] E(2) is the energy of hyperconjugative interactions.
[b] Energy difference between donor (i) and acceptor (j) NBO.
[c] $F(i,j)$ is the Fock matrix element between i and j NBO.

Table 7
Mulliken and natural atomic charges of fentrazamide.

Atoms	Mulliken	Natural	Atoms	Mulliken	Natural
C1	−0.166752	0.77955	N23	−0.170933	−0.01977
C2	0.299129	0.83538	N24	0.482364	−0.32287
C3	−1.072138	0.10928	H25	0.228740	0.22561
C4	−0.013080	−0.02004	H26	0.163008	0.21357
C5	−0.079536	−0.21422	H27	0.190210	0.21471
C6	−0.572120	−0.17262	H28	0.193996	0.22612
C7	−0.204504	−0.19683	H29	0.136948	0.20919
C8	0.305680	−0.16108	H30	0.161552	0.19216
Cl9	0.546423	0.02972	H31	0.190100	0.20829
C10	−1.158834	−0.00479	H32	0.188983	0.20296
C11	−0.084181	−0.39010	H33	0.143253	0.19004
C12	−0.453282	−0.37913	H34	0.174257	0.20192
C13	−0.517182	−0.38179	H35	0.125513	0.18622
C14	−0.299209	−0.38085	H36	0.114337	0.19405
C15	0.131605	−0.39593	H37	0.179369	0.20364
C16	−0.048021	−0.17253	H38	0.242582	0.23481
C17	−0.457388	−0.58484	H39	0.128386	0.18493
O18	−0.233604	−0.59240	H40	0.225961	0.21485
O19	−0.230388	−0.61594	H41	0.129748	0.19390
N20	0.417154	−0.48862	H42	0.142564	0.19521
N21	−0.078794	−0.37030	H43	0.192556	0.22128
N22	0.254296	−0.00602	H44	0.151234	0.20326

and orange-colored surfaces correspond to the negative electrostatic potential regions, while the light-blue and blue regions represent the positive electrostatic potential regions. The green regions indicate where the electrostatic potential is zero. The positive (i.e. blue) and negative (i.e. red) regions indicate the nucleophilic and electrophilic reactive attack sites of molecule, respectively. The MESP surface of fentrazamide was mapped using the B3LYP/6–311++G(d,p) theoretical level. Fig. 6 presents MESP surface map of fentrazamide. The red regions on this map were formed on the O18, O19, N22 and N23 atoms, which are the electrophilic reactive attack sites. Their negative electron density values are $-5.580\ e^{-2}$ for the O18 atom, $-4.703\ e^{-2}$ for the O19 one, $-4.289\ e^{-2}$ for the N22 one and $-3.655\ e^{-2}$ for the N23 one. The positive of fentrazamide are localized around hydrogen atoms, which are nucleophilic reactive attack sites.

4.9. NLO analysis

Nonlinear optical (NLO) phenomena result from the interaction between the electric field component of a high intensity electromagnetic radiation and the electrons of any electronic structure under investigation. Due to the high intensity of the light, a nonlinear polarization occurs in the material and the material exhibits a NLO property. As a result of this light-matter interaction, shifts to high frequency values can be observed and thus very short wavelengths can be reached. Therefore, the research for high-performance NLO materials has become a popular topic in optics. NLO materials play an important role in the design of new optical devices by governing optical processes within photonic systems and technologies. In addition, NLO materials are used in lasers, quantum optics and computing, optical computing, signal processing, data storage, imaging, optical sensing, electro-optic modulators, optical fiber communication, optical switches, high resolution spectroscopy, photodynamic therapy [57–59].

In this study, the parameters such as the polarizability (α), first-order hyperpolarizability (β) and second-order hyperpolarizability (γ) were theoretically analyzed to understand the NLO profile of fentrazamide. Theoretical NLO response was study at the static ($\omega = 0.0$ nm) and frequency-dependent dynamic ($\omega = 532$ nm and 1064 nm) states. The $\alpha_0(0;0)$, $\Delta\alpha(0;0)$, $\beta_0(0;0,0)$ and $\gamma_0(0;0,0,0)$ parameters computed at the static state were listed in Table 8, while the $\alpha_0(-\omega;\omega)$, $\Delta\alpha(-\omega;\omega)$, $\beta_0(-\omega;\omega,0)$ (electro-optical Pockels effect (EOPE)), $\beta_0(-2\omega;\omega,\omega)$ (second harmonic generation (SHG)), $\gamma_0(-\omega;\omega,0,0)$ (electro-optical Kerr effect (EOKE)) and $\gamma_0(-2\omega;\omega,\omega,0)$ (electric-field induced second harmonic generation (EFISHG)) quantities given in Table 9 were presented as the frequency-dependent NLO parameters. Moreover, the projection of the first-order hyperpolarizability $\boldsymbol{\beta}_0$ on the dipole moment vector $\boldsymbol{\mu}_0$, $\beta_{prj.}$ (or $\beta_{vec.}$), was computed for both states. The following equations are used to calculate these mentioned parameters [60].

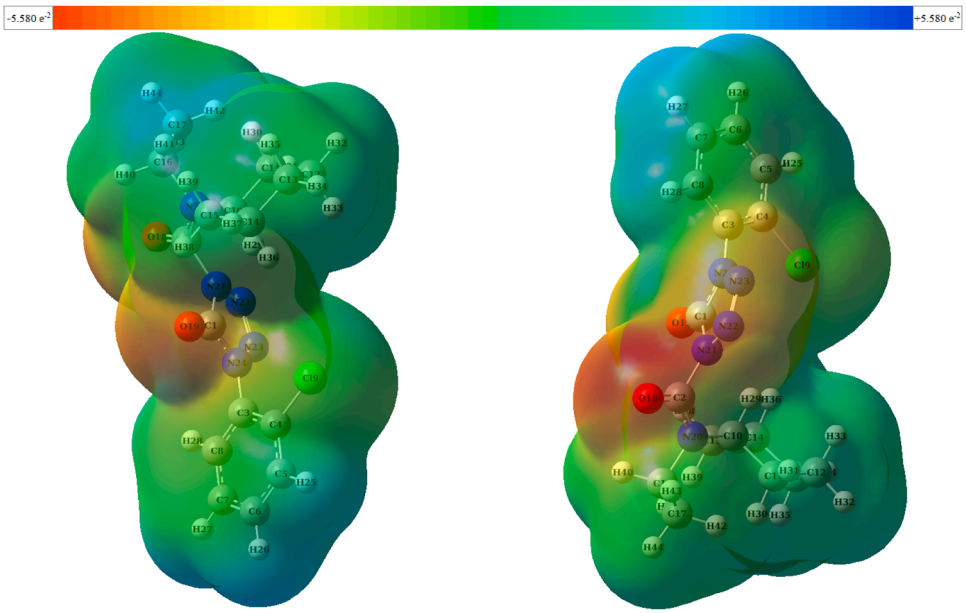

Fig. 6. The simulated MEP surface map of fentrazamide at two different viewing positions.

Table 8
The static dipole moment, polarizability and hyperpolarizability values of fentrazamide.

Parameters (a.u.)	Values
μ_0	1.344340
μ_x	0.272647
μ_y	1.294268
μ_z	0.240386
$\alpha_0(0;0)$	239.85667
$\Delta\alpha(0;0)$	107.33768
$\beta_0(0;0,0)$	304.53352
$\beta_x(0;0,0)$	−266.81790
$\beta_y(0;0,0)$	144.92394
$\beta_z(0;0,0)$	23.36508
$\beta_{prj.}(0;0,0)$	89.59030
$\gamma_0(0;0,0,0)$	3.689286×10^4
$\gamma_x(0;0,0,0)$	3.083444×10^4
$\gamma_y(0;0,0,0)$	1.626996×10^4
$\gamma_z(0;0,0,0)$	1.206686×10^4

Table 9
The frequency dependent polarizability and hyperpolarizability values of fentrazamide.

Parameters (a.u.)	**ω = 532 nm**	**ω = 1064 nm**
$\alpha_0(-\omega;\omega)$	251.22433	242.49167
$\Delta\alpha(-\omega;\omega)$	119.02611	109.95661
$\beta_0(-\omega;\omega,0)$	468.11992	337.49364
$\beta_x(-\omega;\omega,0)$	−415.97300	−298.32317
$\beta_y(-\omega;\omega,0)$	212.16477	155.79746
$\beta_z(-\omega;\omega,0)$	32.99743	25.14747
$\beta_{prj.}(-\omega;\omega,0)$	125.79869	93.98791
$\beta_0(-2\omega;\omega,\ \omega)$	2241.28749	417.59163
$\beta_x(-2\omega;\omega,\ \omega)$	−2152.37563	−370.18527
$\beta_y(-2\omega;\omega,\ \omega)$	581.47957	190.93703
$\beta_z(-2\omega;\omega,\ \omega)$	229.19483	29.81085
$\beta_{prj.}(-2\omega;\omega,\ \omega)$	164.27582	114.07808
$\gamma_0(-\omega;\omega,0,0)$	5.052379×10^4	3.996298×10^4
$\gamma_x(-\omega;\omega,0,0)$	4.350404×10^4	3.356802×10^4
$\gamma_y(-\omega;\omega,0,0)$	2.079289×10^4	1.742367×10^4
$\gamma_z(-\omega;\omega,0,0)$	1.508998×10^4	1.290904×10^4
$\gamma_0(-2\omega;\omega,\omega,0)$	2.377057×10^5	4.647831×10^4
$\gamma_x(-2\omega;\omega,\omega,0)$	2.305123×10^5	3.968715×10^4
$\gamma_y(-2\omega;\omega,\omega,0)$	5.099957×10^5	1.954226×10^4
$\gamma_z(-2\omega;\omega,\omega,0)$	2.685163×10^5	1.425705×10^4

$$\mu_0 = \sqrt{\mu_x^2 + \mu_y^2 + \mu_z^2}$$

$$\alpha_0 = \frac{1}{3}\left(\alpha_{xx} + \alpha_{yy} + \alpha_{zz}\right)$$

$$\Delta\alpha = \frac{1}{\sqrt{2}}\sqrt{\left(\alpha_{xx} - \alpha_{yy}\right)^2 + \left(\alpha_{yy} - \alpha_{zz}\right)^2 + \left(\alpha_{zz} - \alpha_{xx}\right)^2 + 6\alpha_{xz}^2 + 6\alpha_{xy}^2 + 6\alpha_{yz}^2}$$

$$\beta_0 = \sqrt{\beta_x^2 + \beta_y^2 + \beta_z^2} \quad and \quad \beta_{prj.} = \sum_i \frac{\mu_i \beta_i}{|\mu_0|}, \quad \beta_i = \frac{1}{3}\sum_j \left(\beta_{ijj} + \beta_{jij} + \beta_{jji}\right) \quad i,j = \{x,y,z\}$$

$$\gamma_0 = \sqrt{\gamma_x^2 + \gamma_y^2 + \gamma_z^2}, \qquad \gamma_i = \frac{1}{15}\sum_j \left(\gamma_{ijji} + \gamma_{ijij} + \gamma_{iijj}\right) \quad i,j = \{x,y,z\}$$

The magnitude of the dipole moment of fentrazamide is 1.344340 Debye. The calculated $\alpha_0(0;0)$, $\Delta\alpha(0;0)$, $\beta_0(0;0,0)$, $\beta_{prj.}(0;0,0)$ and $\gamma_0(0;0,0,0)$ values of fentrazamide in the static state were obtained as 239.85667 a.u., 107.33768 a.u., 304.53352 a.u. 89.59030 a.u. and 3.689286 × 10^4 a.u., respectively. Similarly, the $\alpha_0(-\omega;\omega)$, $\Delta\alpha(-\omega;\omega)$, $\beta_0(-\omega;\omega,0)$, $\beta_{prj.}(-\omega;\omega,0)$, $\beta_0(-2\omega;\omega,\ \omega)$, $\beta_{prj.}(-2\omega;\omega,\ \omega)$, $\gamma(-\omega;\omega,\ 0,0)$ and $\gamma_0(-2\omega;\omega,\ \omega,0)$ values were found as 251.22433, 119.02611, 468.11992, 125.79869, 2241.28749, 164.27582, 5.052379 × 10^4 and 2.377057 × 10^5 a.u. for ω = 532 nm and 242.49167, 109.95661, 337.49364, 93.98791, 417.59163, 114.07808, 3.996298 × 10^4 and 4.647831 × 10^4 a.u. for ω = 1064 nm, respectively. As can be seen from these results, there is not much difference between the data obtained at the lower frequency ω = 1064 nm and the data found at static ω = 0.0 nm for α, β and γ quantities. A similar situation applies to the $\alpha_0(-\omega;\omega)$, $\Delta\alpha(-\omega;\omega)$, $\beta_0(-\omega;\omega,\ 0)$, $\beta_{prj.}(-\omega;\omega,\ 0)$, $\beta_{prj.}(-2\omega;\omega,\ \omega)$ and $\gamma(-\omega;\omega,\ 0,0)$ calculated at the higher and lower frequency values. However, the $\beta_0(-2\omega;\omega,\ \omega)$ and $\gamma_0(-2\omega;\omega,\ \omega,0)$ parameters computed at the higher frequency ω = 532 nm gave remarkable results comparable to those at both the static and the lower frequency ω = 1064 nm. The computed values at ω = 532 nm for these two parameters are 5.37 and 5.11 times bigger than those at ω=1064 nm.

4.10. Thermochemistry analysis

Knowledge of the thermodynamic parameters of a molecule plays an important role in characterizing its thermal properties in physical and chemical reaction processes. In this context, the thermochemical parameters of fentrazamide were calculated with the B3LYP/6–311++*G* (d,p) at a pressure of 1 atm, a temperature of 298.15 Kelvin and the gas phase state of the molecule. The thermochemical parameters calculated on the basis of the four partition functions (vibrational, rotational, translational and electronic) used by the Gaussian software are summarized in Table 10. The quantities such as entropy, enthalpy, heat capacity, thermal energy and molecular total energy are obtained from the sum of the individual contributions of these four partial functions. The total molecular energy values computed for fentrazamide was found

Table 10
The thermochemical parameters computed of fentrazamide.

Parameters	Values
Rotational temperatures (K)	
T_A	0.01819
T_B	0.00695
T_C	0.00557
Rotational constants (GHz)	
R_A	0.37900
R_B	0.14471
R_C	0.11600
E_{total} (Hartree)	−1506.438755
Zero-point vibrational energy (kcal/mol)	222.97077
Zero-point correction (Hartree/particle)	0.355327
Thermal correction to energy (Hartree/particle)	0.377337
Thermal correction to enthalpy (Hartree/particle)	0.378281
Thermal correction to Gibbs free energy (Hartree/particle)	0.301270
Sum of electronic and zero-point energies (Hartree)	−1506.083429
Sum of electronic and thermal energies (Hartree)	−1506.061419
Sum of electronic and thermal enthalpies (Hartree)	−1506.060474
Sum of electronic and thermal free energies (Hartree)	−1506.137485
$E_{therm.}$ (kcal/mol)	
Total	236.782
Electronic	0.000
Translational	0.889
Rotational	0.889
Vibrational	235.005
C_v (cal/mol × *K*)	
Total	83.521
Electronic	0.000
Translational	2.981
Rotational	2.981
Vibrational	77.560
S (cal/mol × *K*)	
Total	162.082
Electronic	0.000
Translational	43.445
Rotational	35.179
Vibrational	83.458

as −1506.438755 Hartree. The zero-point vibrational energy for fentrazamide was calculated as 222.97077 kcal/mol. The entropy (S), heat capacity (C_v) and thermal energy ($E_{therm.}$) terms were obtained as 162.082 cal/mol × *K*, 83.521 cal/mol × *K* and 236.782 kcal/mol, respectively. As can be seen from Table 10, the biggest contributions within these values come from the individual values of the vibrational partition function. the vibrational partition function contributions are 83.458 cal/mol × *K* for the entropy, 77.560 cal/mol × *K* for the heat capacity and 235.005 kcal/mol for the thermal energy. Three rotational constant values for fentrazamide were detected as 0.37900 GHz for R_A, 0.14471 GHz for R_B and 0.11600 GHz for R_C.

5. Conclusion

The structural, spectroscopic, electronic, NLO and thermodynamic features of a herbicide fentrazamide (4-(2-Chlorophenyl)-*N*-cyclohexyl-*N*-ethyl-4,5-dihydro-5-oxo-1*H*-tetrazole-1-carboxamide or 4-(2-chlorophenyl)-*N*-cyclohexyl-*N*-ethyl-5-oxotetrazole-1-carboxamide) were investigated as both the experimental (FT-IR, UV–Vis. and NMR) and the computational (DFT/B3LYP/6–311++*G*(d,p)). The characteristic C = O and *N* = *N* bonds in the oxotetrazole (tetrazol-5-one) and carboxamide groups of the compound were computed at 1.2099 Å for the C1=O19 bond length, 1.2115 Å for the C2=O18 one, 1.2617 Å for the N22=N23 one in a good harmony with the literature data, while their vibrational frequency values were obtained at 1706, 1751 and 1452 cm^{-1} as the experimental and 1732.1, 1695.8 and 1459.7 cm^{-1} as the theoretical, respectively. The NMR chemical shift analysis was performed for all carbon and hydrogen atoms within fentrazamide. The carbonyl C1 and C2 carbons were found at 147.3 ppm (exp.) and 154.9/154.8 ppm (calc.). The electronic transition features found by the experimental (at 193 and 237 nm) and computational UV–Vis. analyses were supported by electron localizations simulated with HOMO-LUMO plots, and the nature and existence of the intramolecular π→π* and n→π* electronic transitions were revealed. According to the results of the NBO analysis, the strongest hypercoagulative interactions were found for values of σ(C3-C8)→σ*(C3-C4) (5.37 kcal/mol), σ(N21-N22)→π*(C1-O19) (3.20 kcal/mol), π(C5-C6)→π*(C3-C4) (22.45 kcal/mol), n(N24)→σ*(C1-O19) (50.65 kcal/mol) and n(N20)→π*(C2-O18) (69.33 kcal/mol). The negative electrostatic potential regions were found to be −5.580 −4.703, −4.289 and −3.655 e^{-2} on the O18, O19, N22 and N23 atoms, respectively. The NLO behavior of the compound was studied at static and frequency dependent dynamic states. The polarizability (α), first-order hyperpolarizability (β) and second-order hyperpolarizability (γ) values computed at the static and dynamic $\omega = 1064$ nm are very close to each other, while the results at dynamic $\omega = 532$ nm (especially for the $\beta_0(-2\omega;\omega,\ \omega)$ and $\gamma_0(-2\omega;\omega,\ \omega,0)$ quantities) show that the fentrazamide can exhibit a significantly better NLO behavior compared to the other results mentioned. The atomic charges and thermochemical quantities were analyzed by the theoretical modelling.

CRediT authorship contribution statement

Semiha Bahçeli: Writing – original draft, Supervision, Methodology, Investigation, Conceptualization. **Halil Gökce:** Writing – review & editing, Writing – original draft, Visualization, Methodology, Investigation, Formal analysis, Conceptualization.

Declaration of competing interest

The authors declare that they have no known competing financial interests or personal relationships that could have appeared to influence the work reported in this paper.

Data availability

Data will be made available on request.

Supplementary materials

Supplementary material associated with this article can be found, in the online version, at doi:10.1016/j.molstruc.2024.140194.

References

[1] S. Tandon, A. Pujari, N.K. Sand, Degradation of Fentrazamide Herbicide in Soil Under Aerobic Condition, Bull. Environ. Contam. Toxicol. 89 (2012) 312–315.
[2] K. Noda, Competitive effects of barnyardgrass (Echinochloa crus-galli) on rice, in: Proceedings of the 4th Asian-Pacific Weed Science Conference (Rotorua, New Zealand), Asian-Pacific Weed Science Society, 1973, pp. 145–150.
[3] R.J. Smith Jr, Weed competition in rice, Weed Sci 16 (2) (1968) 252–255.
[4] Y. Singh, G. Singh, D. Johnson, M. Mortimer, Changing from transplanted rice to direct seeding in the rice-wheat cropping system in India, in: Rice is life: scientific perspectives for the 21st century. Proceedings of the World Rice Research Conference held in Tsukuba, Japan, 4-7, November 2004, pp. 198–201.
[5] M. Miyahara, Weeds and Their Control in Paddy, Zenkoku Noson Kyoiku Kyokai, Tokyo, 1992 (in Japanese).
[6] T. Goto, S. Ito, A. Yanagi, Y. Watanabe, K. Yasui, Studies on herbicidal carbamoyltetrazolinone derivatives: selection of fentrazamide, Weed Biol. Manage. 2 (1) (2002) 18–24.
[7] A. Yanagi, Y. Watanabe, S. Narabu, S. Ito, T. Goto, Synthesis and herbicidal activity of 1-(sub.) phenyl-5-carbamoyltetrazolinone derivatives: synthesis of fentrazamide, J. Pestic. Sci. (Japan) 26 (2001) 62.
[8] T. Goto, A. Yanagi, Y. Watanabe, Inhibition of Cell Division (Oxyacetamides, Tetrazolinones), in: W. Kramer, U. Schirmer (Eds.), Modern Crop Protection Compounds Volume 1, Wiley-VCH Verlag GmbH & Co, KGaA, Weinheim, Germany, 2007 325334.
[9] J. Shekhar, B.S. Mankotia, A.D. Bindra, Bio-efficacy of some new herbicides against weed in transplanted rice (Oryza sativa L), Ind. J. Weed. Sci. 36 (1,2) (2004) 50–53.
[10] G. Schmuck, A. Freyberger, H.-J. Ahr, B. Stahl, M. Kayser, Effects of the New Herbicide Fentrazamide on the Glucose Utilization in Neurons and Erythrocytes In Vitro, Neurotoxicology 24 (2003) 55–64.
[11] A. Yanagi, Y. Watanabe, S. Narabu, S. Ito, T. Goto, Development of a New Herbicide, Fentrazamide, J. Pestic. Sci. 27 (2) (2002) 199–209.
[12] I. Mukherjee, M. Gopal, Evaluation of Fentrazamide for Weed Control and Estimation of its Residues in Rice, Bull. Environ. Contam. Toxicol. 74 (2005) 667–672.
[13] S.J. Lim, Y. Sunohara, H. Matsumoto, Action of fentrazamide on protein metabolism and cell division in plants, J. Pestic. Sci. 32 (3) (2007) 249–254.
[14] T. Goto, S. Ukawa, H. Miyauchi, Fentrazamide-a new herbicide effective on grasses and annual sedges in rice in Japan, Pflanzenschutz Nachr Bayer 54 (1) (2001) 13–34.
[15] P. Böger, Mode of action for chloroacetamides and functionally related compounds, J. Pestic. Sci. (Japan) 28 (3) (2003) 324–329.
[16] S. Ito, C. Ueno, T. Goto, Effect of fentrazamide on the growth, morphology and anatomy of Echinochloa crus-galli and Echinochloa oryzicola, J. Pestic. Sci. (Japan) 33 (3) (2008) 228–233.
[17] S.J. Lim, Y. Sunohara, H. Matsumoto, Absorption, translocation, and metabolism of fentrazamide in rice and early watergrass (Echinochloa oryzicola), Weed Biol. Manag. 8 (2008) 215–218.
[18] T. Goto, S. Ito, A. Yanagi, Y. Watabane, K. Yasu, Studies on herbicidal carbamoyltetrazolinone derivatives: selection of fentrazamide, Weed Biol. Manag. 2 (2002) 18–24.
[19] S. Tandon, A. Pujari, N.K. Sand, Dissipation studies of fentrazamide (YRC-2388) in soil under anaerobic condition, J. Environ. Monit. 14 (2012) 2521–2526.
[20] S. Tandon, A. Pujari, N.K. Sand, Degradation of Fentrazamide Herbicide in Soil Under Aerobic Condition, Bull. Environ. Contam. Toxicol. 89 (2012) 312–315.
[21] A.D. Becke, Density-functional thermochemistry. III. The role of exact Exchange, J. Chem. Phys. 98 (7) (1993) 5648–5652.
[22] C. Lee, W. Yang, R.G. Parr, Development of the Colle-Salvetti correlation-energy formula into a functional of the electron density, Phys. Rev. B 37 (2) (1988) 785–789.
[23] M.J. Frisch, G.W. Trucks, H.B. Schlegel HB, G.E. Scuseria, et al., Gaussian 09, Revision C.01, Gaussian Inc, Wallingford, CT, 2009.
[24] R. Dennington, T. Keith, J. Millam, GaussView, Version 5, Semichem Inc, Shawnee Mission KS, 2009.
[25] N. Sundaraganesan, S. Ilakiamani, H. Saleem, Piotr.M. Wojciechowski, D. Michalska, FT-Raman and FT-IR spectra, vibrational assignments and density functional studies of 5-bromo-2-nitropyridine, Spectrochim. Acta A Mol. Biomol. Spectrosc. 61 (2005) 2995–3001.
[26] M.H. Jamr'oz, Vibrational Energy Distribution Analysis VEDA4, Warsaw, 2004.
[27] M.H. Jamr'oz, Vibrational energy distribution analysis (VEDA): scopes and limitations, Spectrochim. Acta A Mol. Biomol. Spectrosc. 114 (2013) 220–230.
[28] E. Runge, E.K.U. Gross, Density-Functional Theory for Time-Dependent Systems, Phys. Rev. Lett. 52 (12) (1984) 997–1000.
[29] F. London, Théorie Quantique des Courants Interatomiques dans les Combinaisons Aromatiques, J. Phys. Radium 8 (10) (1937) 397–409.
[30] R. Ditchfield, Self-Consistent Perturbation Theory of Diamagnetism, Mol. Phys. 27 (4) (1974) 789–807.

[31] K. Wolinski, J.F. Hinton, P. Pulay, Efficient Implementation of the Gauge-Independent Atomic Orbital Method for NMR Chemical Shift Calculations, J. Am. Chem. Soc. 112 (23) (1990) 8251–8260.
[32] E. Cancès, B. Mennucci, J. Tomasi, A New Integral Equation Formalism for the Polarizable Continuum Model: theoretical Background and Applications to Isotropic and Anisotropic Dielectrics, J. Chem. Phys. 107 (8) (1997) 3032–3041.
[33] T. Lu, F. Chen, Multiwfn: a multifunctional wavefunction analyzer, J. Comput. Chem. 33 (2012) 580–592.
[34] P. He, J.-G. Zhang, K. Wang, X. Yina, T.-L. Zhang, Computational studies on two novel energetic nitrogen-rich compounds based on tetrazolone, J. Phys. Org. Chem. 29 (2016) 29–34.
[35] X. Yin, J.-T. Wu, X. Jin, C.-X. Xu, P. He, T. Li, K. Wang, J. Qin, J.-G. Zhang, Nitrogen-rich salts of 1-aminotetrazol-5-one: oxygen-containing insensitive energetic materials with high thermal stability, RSC Adv 5 (2015) 60005–60014.
[36] A. Duque-Prata, C. Serpa, P.J.S.B. Caridade, Photochemistry of 1-Phenyl-4-Allyl-Tetrazol-5-One: a Theoretical Study Contribution towards Mechanism Elucidation, Appl. Sci. 11 (2021) 4045.
[37] A. Gomez-Zavaglia, I.D. Reva, L. Frija, M.L. Cristiano, R. Fausto, Photochemistry of 1-phenyl-tetrazolone isolated in solid argon, J. Photochem. Photobiol. A: Chem. 179 (2006) 243–255.
[38] N.B. Colthup, L.H. Daly, E. Wiberley, Introduction to Infrared and Raman Spectroscopy, Academic Press, New York, 1964.
[39] R.M. Silverstein, F.X. Webster, Spectroscopic Identification of Organic Compound, 6th ed, John Willey & Sons, New York, 1998.
[40] B.H. Stuart, Infrared Spectroscopy: Fundamentals and Applications, JohnWilley & Sons, England, 2004.
[41] O. Akyıldırım, H. Gökce, S. Bahçeli, H. Yüksek, Theoretical and spectroscopic (FT-IR, NMR and UV–Vis.) characterizations of 3-p-chlorobenzyl-4-(4-carboxybenzylidenamino)-4,5-dihydro-1H-1,2,4-triazol-5-one molecule, J. Mol. Struct. 1127 (2017) 114–123.
[42] A. Ismael, C. Serpa, M.L.S. Cristiano, Photochemistry of 1-allyl-4-aryltetrazolones in solution; structural effects on photoproduct selectivity, Photochem. Photobiol. Sci. 12 (2013) 272–283.
[43] N.M. O'Boyle, A.L. Tenderholt, K.M. Langner, Software News and Updates cclib: a Library for Package-Independent Computational Chemistry Algorithms, J. Comput. Chem. 29 (2008) 839–845.
[44] E.B. Nielsen, J.A. Schellman, The Absorption Spectra of Simple Amides and Peptides, J. Phys. Chem. 71 (7) (1967) 2297–2304.
[45] K. Fukui, Role of Frontier Orbitals in Chemical Reactions, Science 218 (4574) (1982) 747–754.
[46] R.G. Parr, R.G. Pearson, Absolute Hardness: companion Parameter to Absolute Electronegativity, J. Am. Chem. Soc. 105 (26) (1983) 7512–7516.
[47] R.G. Pearson, Absolute Electronegativity and Hardness: applications to Organic Chemistry, J. Org. Chem. 54 (6) (1989) 1430–1432.
[48] R.G. Parr, L. Szentpaly, S. Liu, Electrophilicity Index, J. Am. Chem. Soc. 121 (9) (1999) 1922–1924.
[49] P. Geerlings, F. De Proft, W. Langenaeker, Conceptual Density Functional Theory, Chem. Rev 103 (5) (2003) 1793–1873.
[50] C.-G. Zhan, J.A. Nichols, D.A. Dixon, Ionization Potential, Electron Affinity, Electronegativity, Hardness, and Electron Excitation Energy: molecular Properties from Density Functional Theory Orbital Energies, J. Phys. Chem. A 107 (20) (2003) 4184–4195.
[51] C. Alaşalvar, N. Öztürk, H. Gökce, A. Güder, E. Menteşe, H. Bektaş, Synthesis, structural, spectral, antioxidant, bioactivity and molecular docking investigations of a novel triazole derivative, J. Biomol. Struct. Dyn. 40 (14) (2022) 6642–6655.
[52] J.-İ. Aihara, Reduced HOMO-LUMO Gap as an Index of Kinetic Stability for Polycyclic Aromatic Hydrocarbons, J. Phys. Chem. A 103 (1999) 7487–7495.
[53] F. Wienhold, C.R. Landis, Valency and Bonding-A Natural Bond Orbital Donor-Acceptor Perspective, Cambridge University Press, New York, 2005.
[54] R.S. Mulliken, Electronic population analysis on LCAO-MO molecular wave functions. I, J. Chem. Phys. 23 (10) (1955) 1833–1840.
[55] A.E. Reed, R.B. Weinstock, F. Weinhold, Natural population analysis, J. Chem. Phys. 83 (2) (1985) 735–746.
[56] C.H. Suresh, G.S. Remya, P.K. Anjalikrishna, Molecular electrostatic potential analysis: a powerful tool to interpret and predict chemical reactivity, WIREs Comput. Mol. Sci. 12 (2) (2022) e1601.
[57] R. Bano, M. Asghar, K. Ayub, T. Mahmood, J. Iqbal, S. Tabassum, R. Zakaria, M. A. Gilani, A Theoretical Perspective on Strategies for Modeling High Performance Nonlinear Optical Materials, Front. Mat. 8 (2021) 783239.
[58] L. Zhou, H. Fu, T. Lv, C. Wang, H. Gao, D. Li, L. Deng, W. Xiong, Nonlinear Optical Characterization of 2D Materials, Nanomaterials 10 (11) (2020) 2263.
[59] H. Gökce, S. Ceylan, N. Öztürk, Y. Sert, Tautomeric, spectroscopic, electronic and NLO analyses of purpald (4-amino-3-hydrazino-5-mercapto-1,2,4-triazole), Mater. Today Commun. 32 (2022) 103862.
[60] H.A. Kurtz, D.S. Dudis, Quantum Mechanical Methods for Predicting Nonlinear Optical Properties, in: K.B. Lipkowitz, D.B. Boyd (Eds.), Reviews in Computational Chemistry, Volume 12, Wiley-VCH, Inc., 1998, pp. 241–279.